

Legends for supplementary tables are provided in the accompanying Excel file, as listed in the supplementary table section.

Contents

| | |
|--|----|
| S1: Fig. S – Supplementary figures | 3 |
| Fig. S1 – Trees individual pictures | 3 |
| Fig. S2 – 10 % hydrochloric acid effervescence reaction on tree species..... | 4 |
| Fig. S3 – CaOx scanning electron microscopy and energy dispersive X-ray spectroscopy | 5 |
| Fig. S4 – Absolute amounts of calcium oxalate..... | 7 |
| Fig. S5 – Counts of phylum specific amplicon sequence variants and relative abundance according to tree species..... | 8 |
| Fig. S6 – Count of phylum specific amplicon sequence variants and relative abundance according to organic matter or soil samples | 9 |
| Fig. S7 – Genus specific relative abundance according to tree species and sample types..... | 10 |
| Fig. S8 – Alpha diversity metrics..... | 11 |
| Fig. S9 – Non-metric multidimensional scaling analysis of the beta diversity between samples of different tree species and different sample types..... | 12 |
| Fig. S10 – Principal component analysis on bulk soil variables | 13 |
| Fig. S11 – X-ray fluorescence of eight major elements by site and parent material..... | 14 |
| Fig. S12 – Soil pH of the different sampling sites and parent materials | 15 |
| S2: Table S – Supplementary table listing | 16 |
| Table S1 – List of species that have evidence of an active oxalate-carbonate pathways | 16 |
| Table S2 – CaOx identification in 25 species present in Sadhana Forest | 16 |
| Table S3 – Size of sampled individuals and biomass values | 16 |
| Table S4 – PCR results and selection of samples for HTS for all microbial samples..... | 16 |
| Table S5 – CaOx content of the species..... | 16 |

| | |
|--|----|
| Table S6 – Adjusted <i>p</i> -values from the PERMANOVA analysis of the <i>frc</i> gene data | 16 |
| Table S7 – Bulk soil properties..... | 16 |
| Table S8 – Concentrations of elements obtained by X-ray fluorescence..... | 16 |
| Table S9 – Data of mineral compositions obtained by X-ray diffraction | 16 |
| Table S10 – Identified oxalotrophic communities and whether they are known or unknown | 16 |
| S3: Methods S – Supplementary methods | 17 |
| S3.1 Parent materials | 17 |
| S3.2 Soil analysis method choices | 17 |
| S3.3 Primer sequences | 17 |
| S3.4 Polymerase chain reaction program..... | 17 |
| S3.5 Sequence analysis..... | 18 |
| S3.6 Alpha and beta diversity statistical analysis | 19 |
| S3.7 Principal Component Analysis | 19 |
| S4: Eq. (S) – Supplementary equations | 21 |
| References | 22 |

S1: Fig. S – Supplementary figures

Fig. S1 – Trees individual pictures



Fig. S1. Sampled trees individuals. *Lepisanthes tetraphylla* (A) L1, (B) L2, (C) L3, (D) L4; *Artocarpus heterophyllus* (E) A1, (F) A2, (G) A3 behind the banana plants, (H) A4; *Sapindus emarginatus* (I) Sa1, (J) Sa2, (K) Sa3, (L) Sa4; *Diospyros ebenum* (M) D1, (N) D2, (O) D3, (P) D4.

Fig. S2 – 10 % hydrochloric acid effervescence reaction on tree species

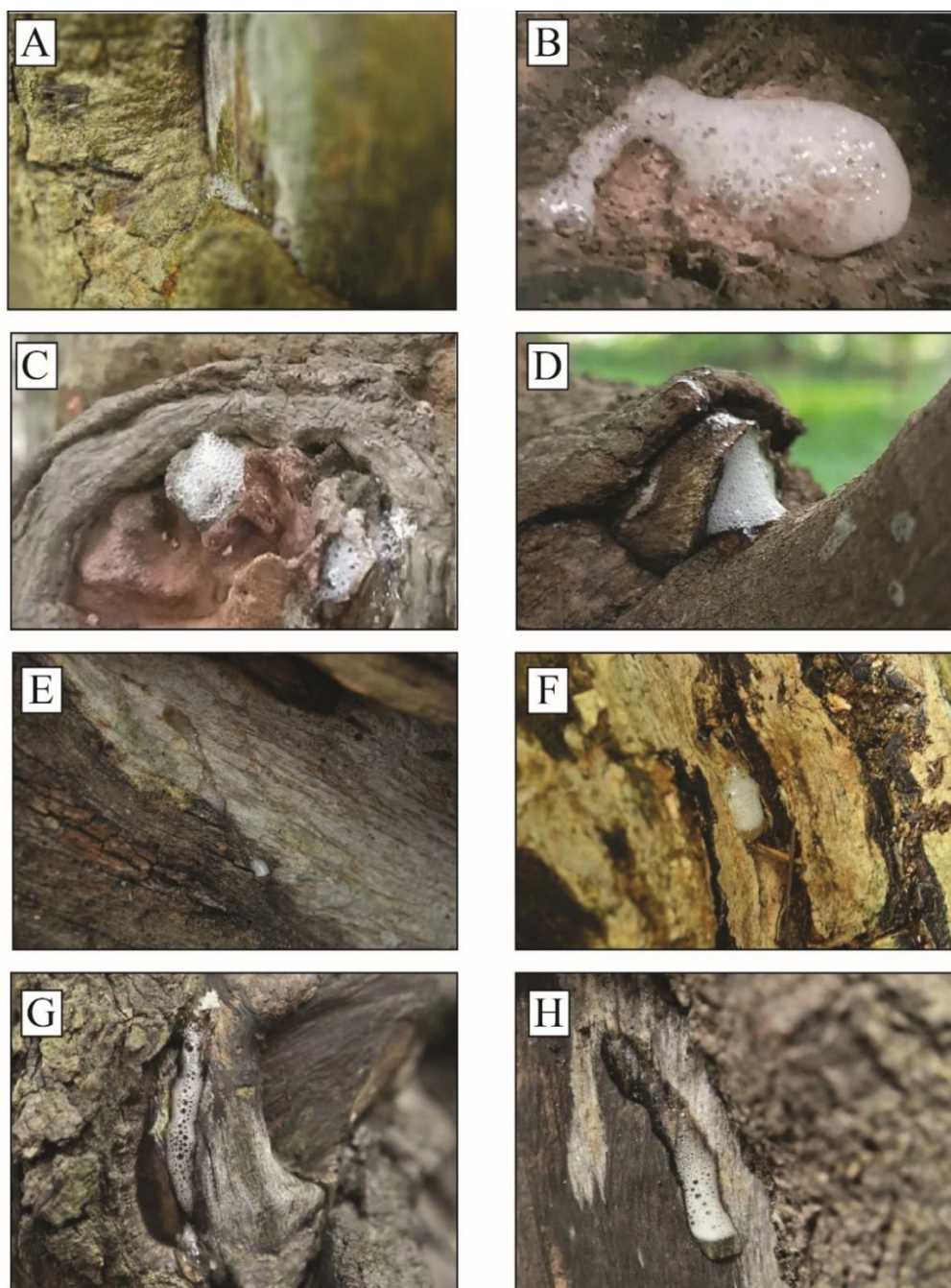
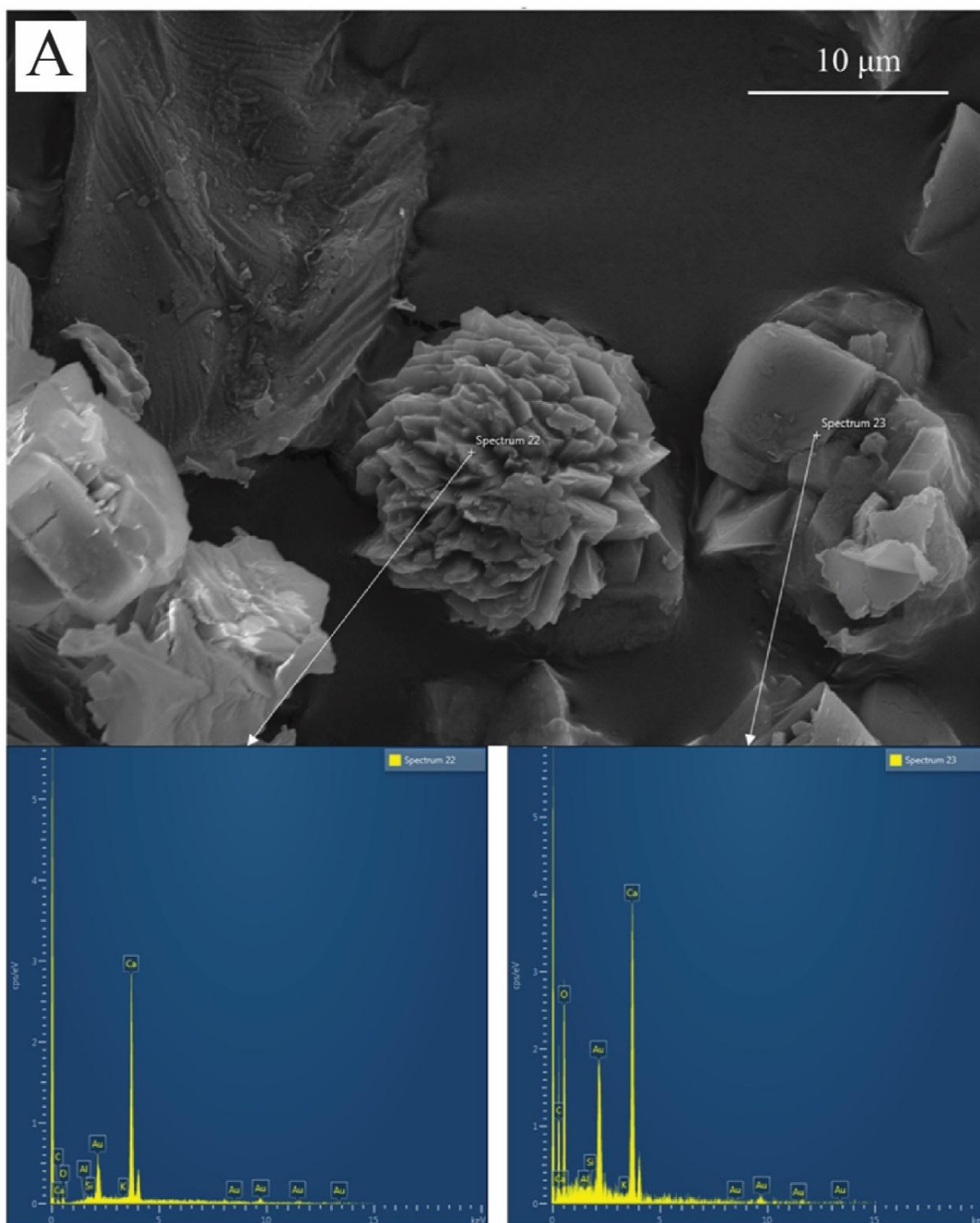


Fig. S2. Photos of reactions observed on different tree species with 10 % hydrochloric acid indicating the presence of calcium carbonate ($2 \text{HCl} + \text{CaCO}_3 = \text{CaCl}_2 + \text{H}_2\text{O} + \text{CO}_2$). (A) *Lepisanthes tetraphylla* trunk. (B) *L. tetraphylla* root. (C) *Artocarpus heterophyllus* trunk. (D) *A. heterophyllus* branch. (E) *Sapindus emarginatus* trunk. (F) *S. emarginatus* branch with traces of phyto-predation. (G) *Diospyros ebenum* branch. (H) *D. ebenum* trunk.

Fig. S3 – CaOx scanning electron microscopy and energy dispersive X-ray spectroscopy



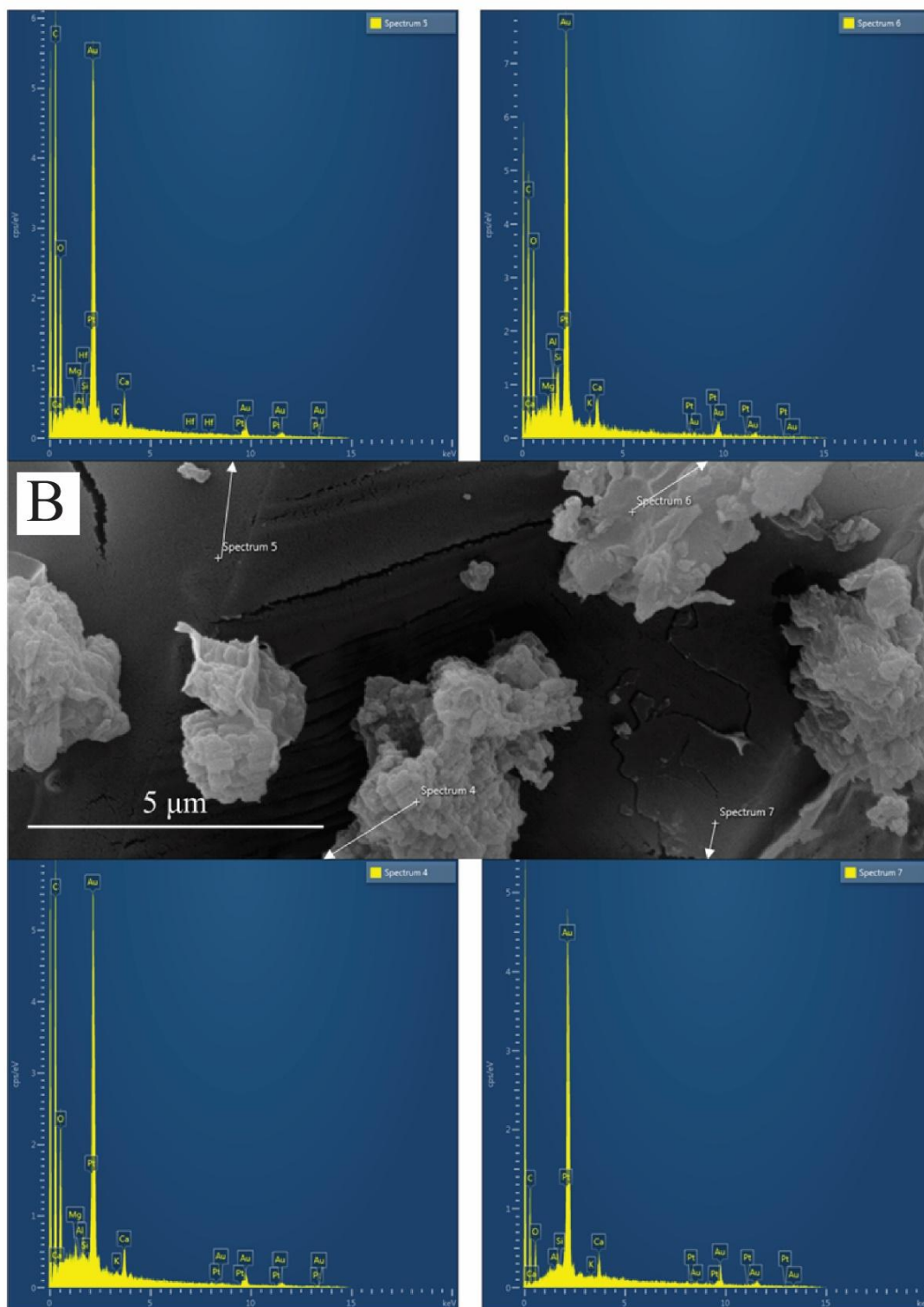


Fig. S3. CaOx SEM and EDX spectroscopy. (A) EDX-spectra from two druses type, showing Calcium and Oxygen peaks. Sample from litter (leaves) of *A. heterophyllum* A4; (B) EDX-spectra of prismatic crystals with micrite (CaCO₃) coatings from *S. emarginatus* Sa3.

Fig. S4 – Absolute amounts of calcium oxalate

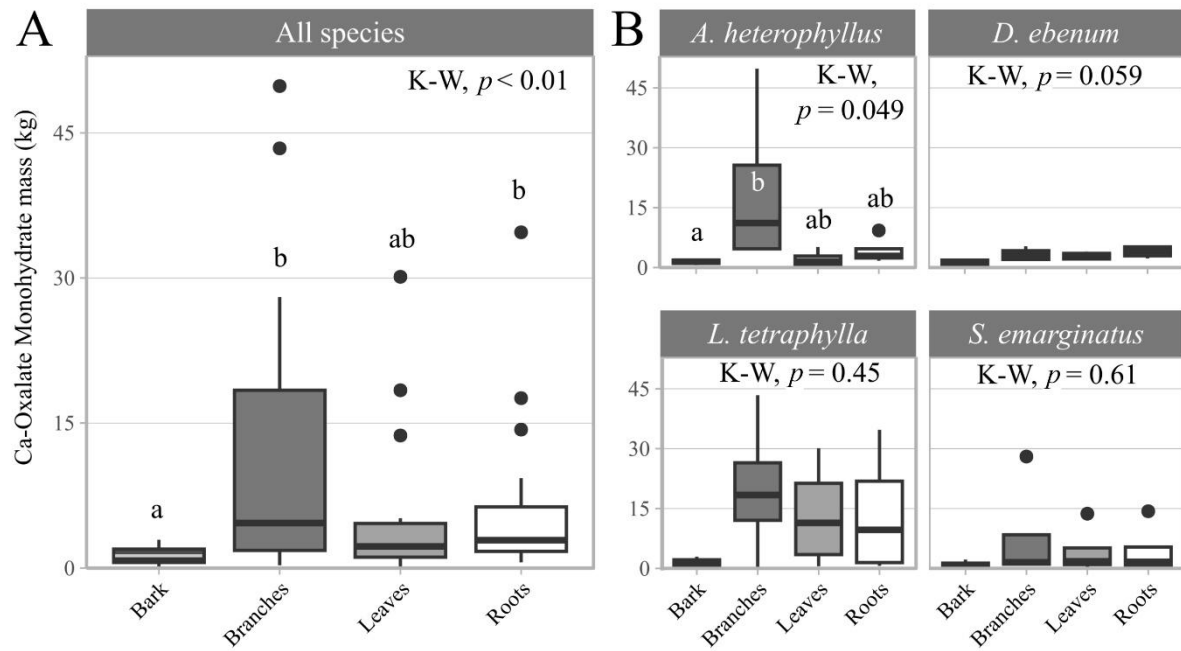


Fig. S4. Boxplots of CaOx absolute amounts. Absolute quantities of calcium oxalate monohydrate within trees, adjusted for the biomass of individuals and plotted as both an average of (A) all tree species and (B) per tree species for each organic matter type.

Fig. S5 – Counts of phylum specific amplicon sequence variants and relative abundance according to tree species

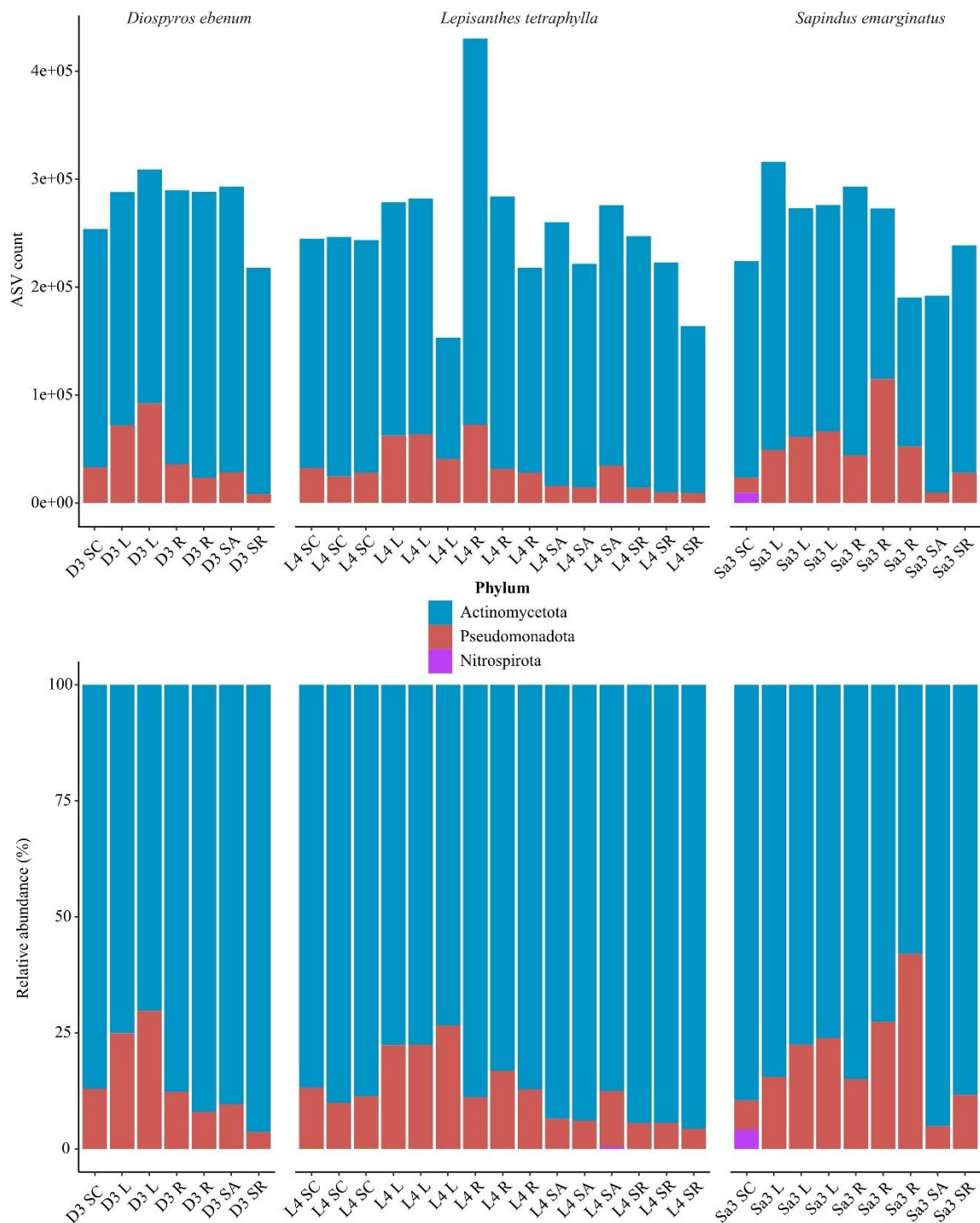


Fig. S5. Counts of phylum specific amplicon sequence variants (ASV) and their relative abundance (%) according to tree species. Samples are listed with the tree sampled (D - *Diospyros ebenum*; L - *Lepisanthes tetraphylla*; Sa - *Sapindus emarginatus*) and then the sample type (SC - control soil; L - litter; R - roots; SA - adjacent soil; SR - rhizosphere soil).

Fig. S6 – Count of phylum specific amplicon sequence variants and relative abundance according to organic matter or soil samples

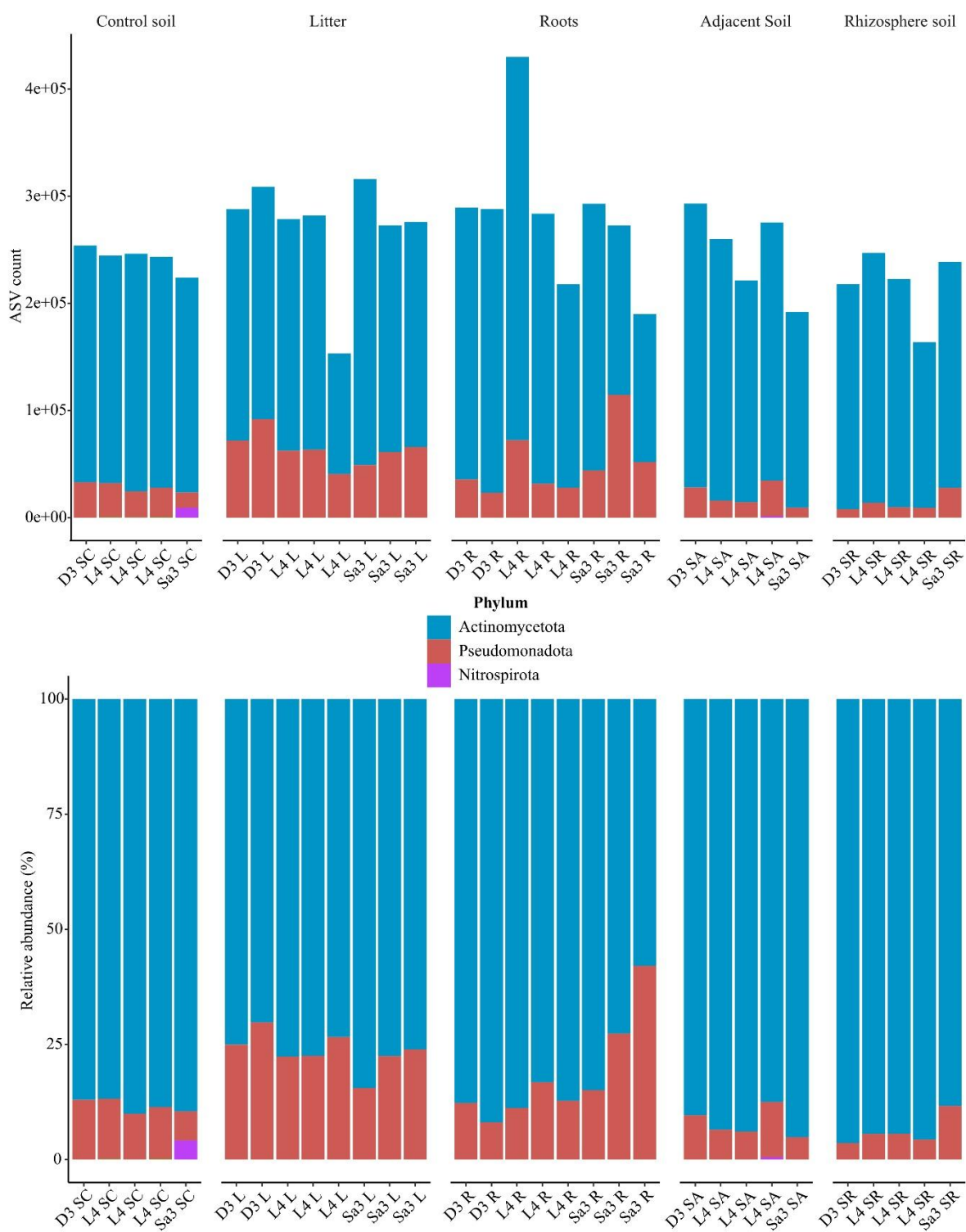


Fig. S6. Counts of phylum specific amplicon sequence variants (ASV) and relative abundance (%) according to sample types. Symbols as in Fig. S5.

Fig. S7 – Genus specific relative abundance according to tree species and sample types

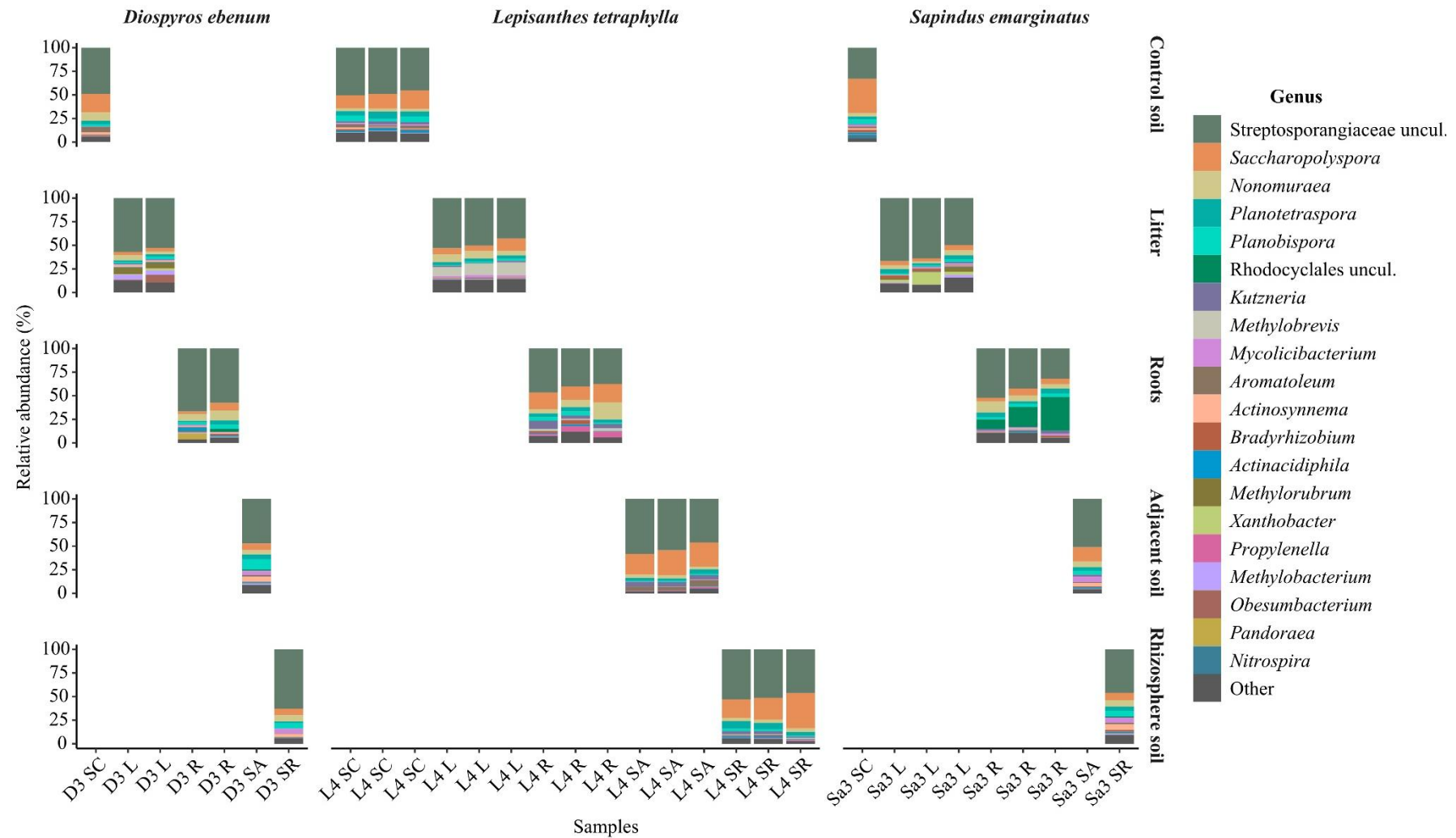


Fig. S7. Genus specific relative abundance (%) according to tree species and sample types. Symbols as in Fig. S5.

Fig. S8 – Alpha diversity metrics

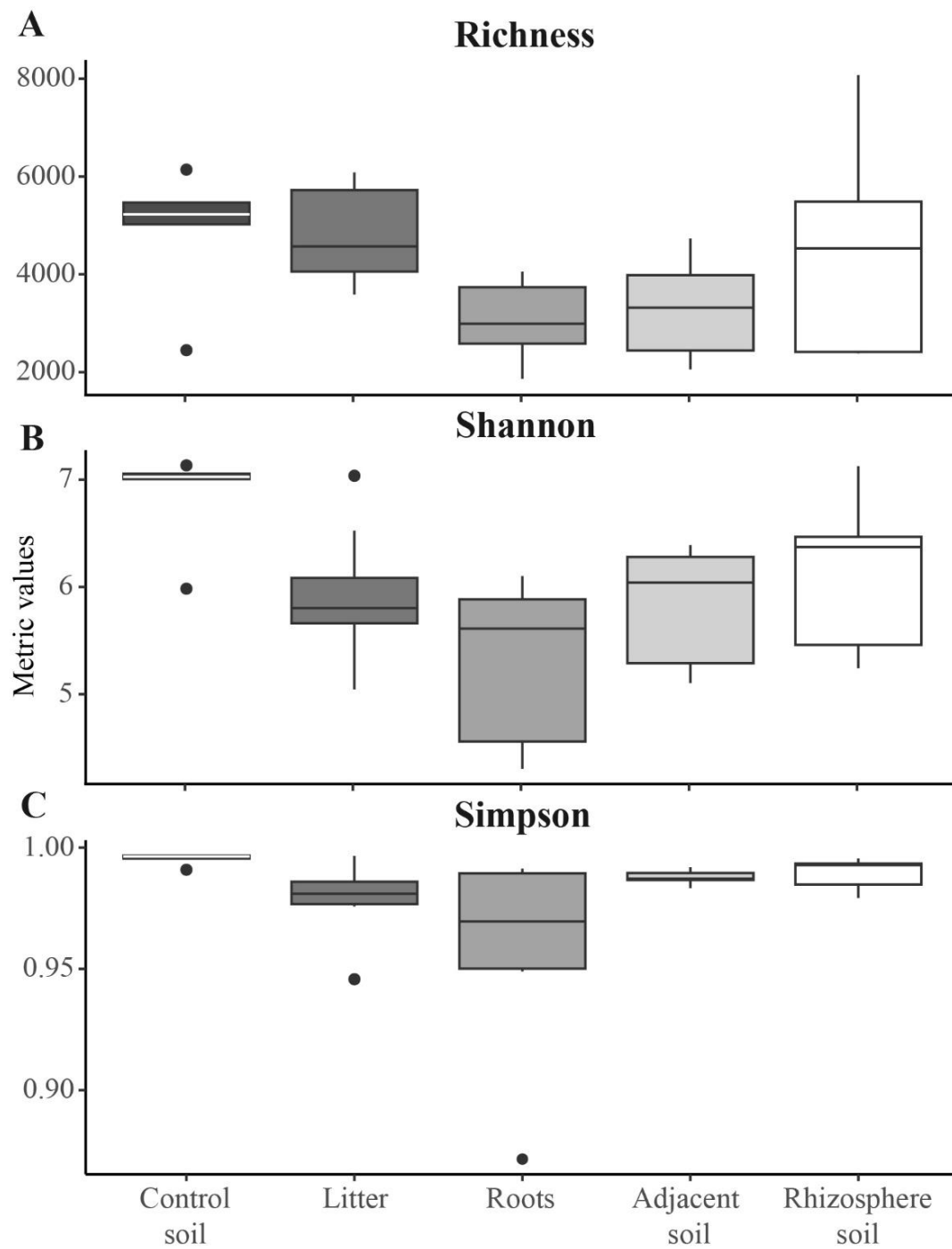


Fig. S8. Alpha diversity metrics including amplicon sequence variants (A) richness, (B) Shannon, and (C) Simpson diversity indices according to sample types. The midline in the box plot represents the median, box extents are the 1st and 3rd quartiles, and whiskers reach 1.5 times the inter-quartile range, while the dots represent outliers, outside of this range.

Fig. S9 – Non-metric multidimensional scaling analysis of the beta diversity between samples of different tree species and different sample types

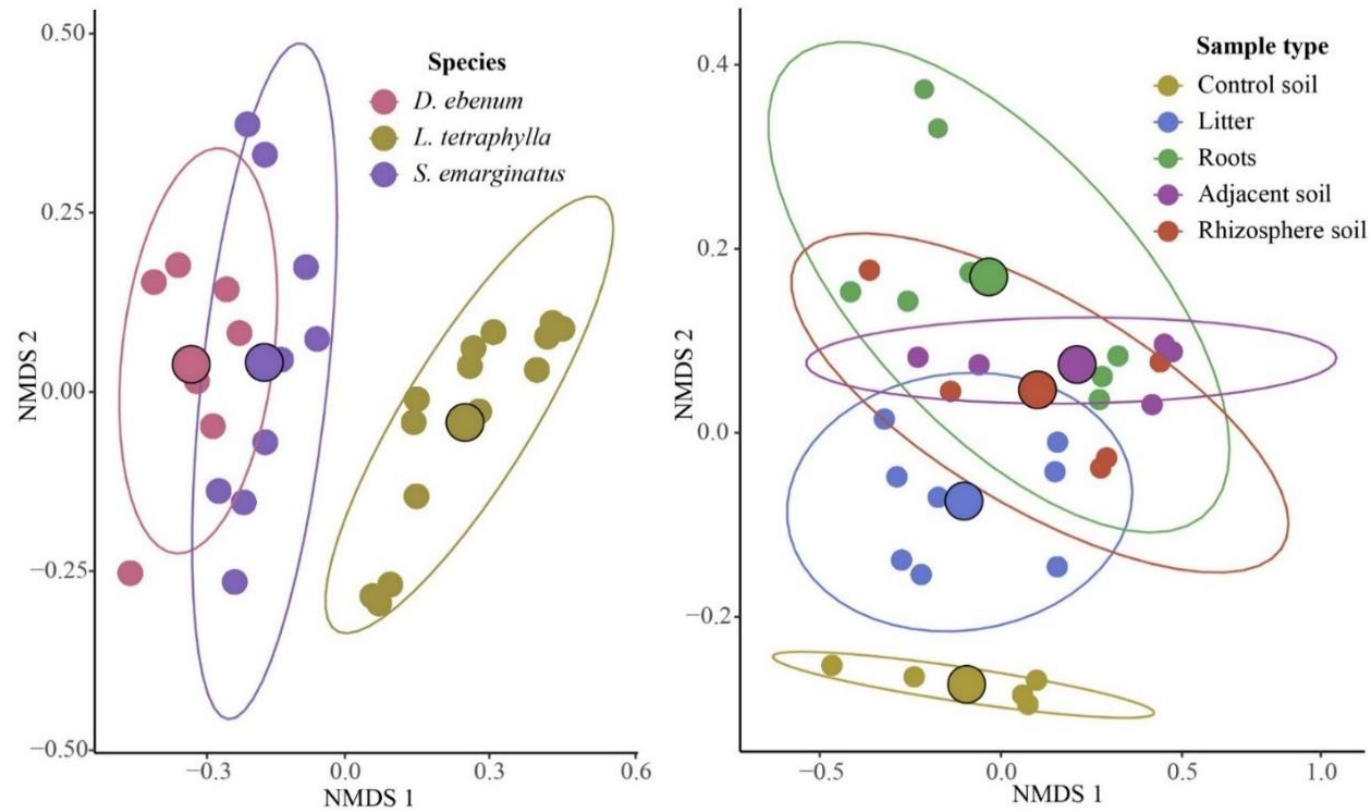


Fig. S9. Non-metric multidimensional scaling analysis based on microbial communities in samples of different tree species and different sample types. The ellipses represent the 95 % confidence interval of the mean values for each group, being either species or sample type. Large dots localize the center of the ellipses.

Fig. S10 – Principal component analysis on bulk soil variables

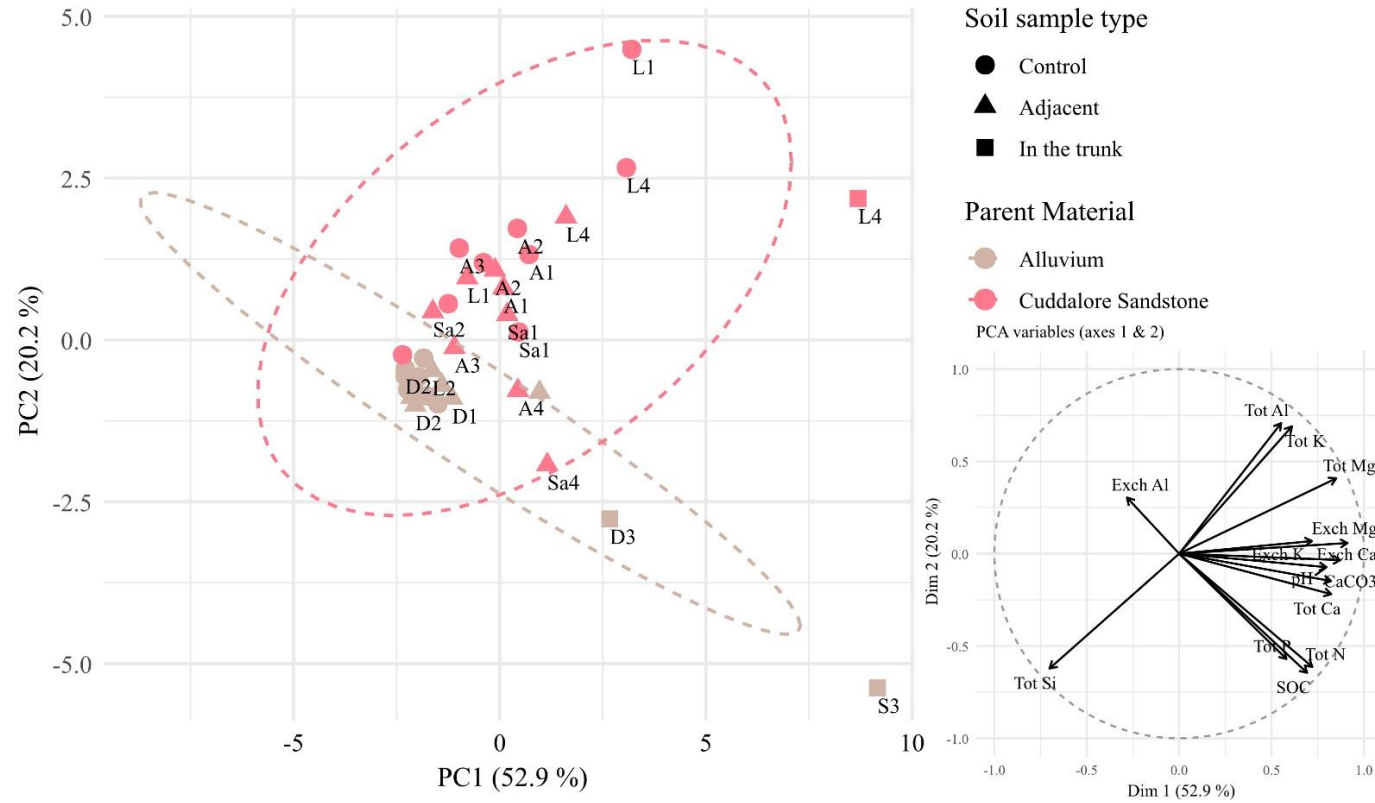


Fig. S10. Principal component analysis (PCA) on the correlation matrix highlighting the similarities among parent materials based on soil variables. Left: ellipses indicate regions where the probability that sample distributions differ within the Euclidian space is statistically significant at $\alpha = 0.05$. **Right:** circle of correlations of variables with principal components 1 and 2. See Methods S3.7 section for more details on the PCA analysis. CaCO₃ – calcium carbonate; Exch Al – Exchangeable aluminium; Exch Ca – Exchangeable calcium; Exch K – Exchangeable potassium; Exch Mg – Exchangeable magnesium; pH; SOC – soil organic carbon; Tot Al – Tot aluminium; Tot Ca – Total calcium; Tot K – Total potassium; Tot Mg – Total magnesium; Tot N – Total nitrogen; Tot P – Total phosphorus; Tot Si – Total silicon.

Fig. S11 – X-ray fluorescence of eight major elements by site and parent material

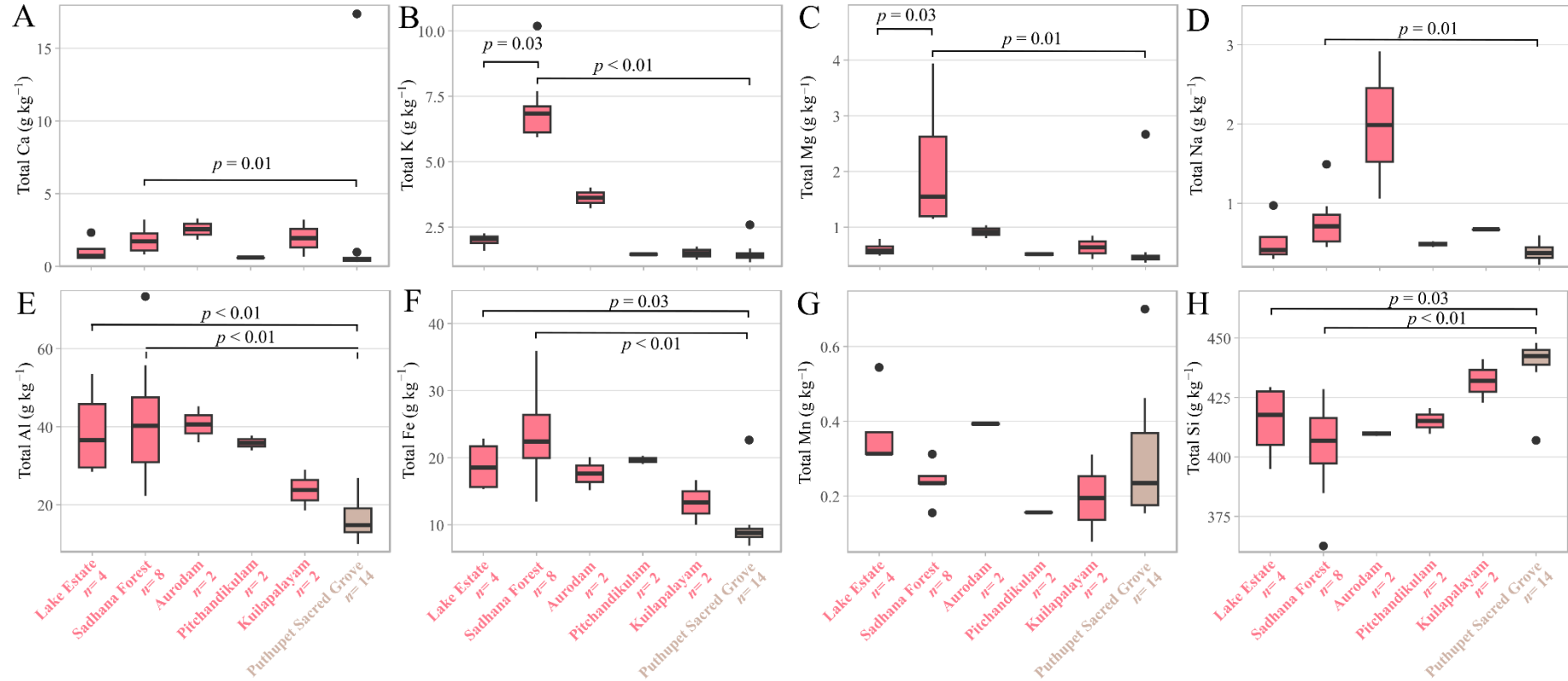


Fig. S11. Concentrations in height major elements (measured using X-ray fluorescence) by site and by parent material (red = Cuddalore sandstone; brown = Alluvium).

(A) Calcium, (B) Potassium, (C) Magnesium, (D) Sodium, (E) Aluminium, (F) Iron, (G) Manganese, (H) Silicon. Horizontal bars represent significant adjusted p -value (< 0.05) after a Wilcoxon signed-rank test.

Fig. S12 – Soil pH of the different sampling sites and parent materials

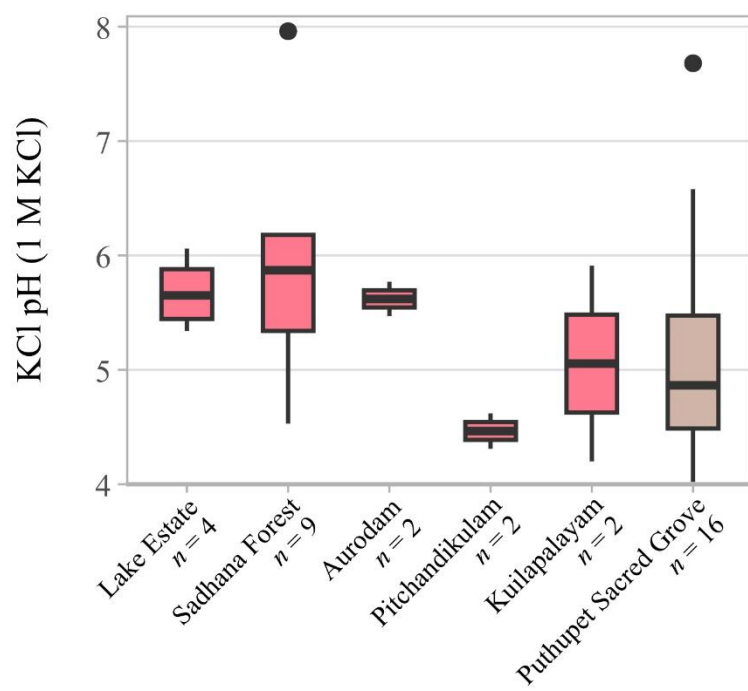


Fig. S12. Soil pH measured in 1 M potassium chloride by site and by parent material (red = Cuddalore sandstone; brown = Alluvium).

S2: Table S – Supplementary table listing

Please refer to the separate Excel file for the supplementary tables. In order:

Table S1 – List of species that have evidence of an active oxalate-carbonate pathways

Papers and theses cited in the table: Garvie 2003, 2006; Cailleau et al. 2011, 2014; Clerc de Sonarc lens 2011; Aragno and Verrecchia 2012; Ferro 2012; Bravo et al. 2015; Rowley et al. 2017; Hervé et al. 2018; Pons et al. 2018; Rande voson 2019; Steinmann 2020; Álvarez-Rivera et al. 2021.

Table S2 – CaOx identification in 25 species present in Sadhana Forest

Papers and theses cited in the table: Sahri et al. 1993; Srivastava et al. 1997; Wallnöfer 2001; Malik et al. 2004; Sharawy 2004; Ibrahim et al. 2006; Jadhav 2009; Paarakh 2009; Alli Smith 2009; Dhale et al. 2010; Chanda et al. 2010; Friday et al. 2011; Akpakpan and Akpabio 2012; Khalid et al. 2015; Prakash et al. 2015; Sharma et al. 2017; Hervé et al. 2018; Pande et al. 2018; Pierantoni et al. 2018.

Table S3 – Size of sampled individuals and biomass values

Table S4 – PCR results and selection of samples for HTS for all microbial samples

Table S5 – CaOx content of the species

Table S6 – Adjusted *p*-values from the PERMANOVA analysis of the *frc* gene data

Table S7 – Bulk soil properties

Table S8 – Concentrations of elements obtained by X-ray fluorescence

Table S9 – Data of mineral compositions obtained by X-ray diffraction

Table S10 – Identified oxalotrophic communities and whether they are known or unknown

S3: Methods S – Supplementary methods

S3.1 Parent materials

The Alluvium formation is a mixture of fluvial Quaternary deposits, transported and deposited by the neighbouring Kaluvelli Swamps, Ponnaiyar or Gingee rivers, with coastal sand dunes (Vincent and Violette, 2017). The underlying Cuddalore sandstone is constituted of permeable iron-rich sandstones, yellow clays, silts, and lignite, and was formed from the deposition of charnokite-alteration products (Eastern Ghats) in a deltaic environment during the late Miocene (5.3–10 Ma; Subramanian et al. 2013). The Manaveli clay formation consists of fine-grained sand- to siltstone with a low permeability, which contains poorly preserved molluscs. This formation was deposited in a shallow sea environment during the Paleocene (56–66 Ma; Sundaram et al. 2001; Vincent and Violette 2017).

S3.2 Soil analysis method choices

Only surficial soil layers were sampled because (i) oxalotrophy may affect biogeochemical processes in surface soils through litter inputs, and (ii) only a limited amount of material could be sent to Switzerland for further analyses. Soil pH_{KCl} used as pre-testing revealed that it was more reproducible than the soil pH in H_2O . Exchangeable cations were extracted with a cobalt hexamine solution because it is less aggressive towards CaCO_3 (Rowley et al., 2020). Loeppert et al. (1984)'s acetic acid method was used to measure CaCO_3 content as it is known to be reliable in soils with low CaCO_3 content (Loeppert and Suarez, 1996), and a pre-testing confirmed that this method is far more reproducible than the calcimeter or mass loss methods applied to the studied soils.

S3.3 Primer sequences

frc171-F (5'-CTSTAYTTCACSATGCTSAAC-3')

frc306-R (5'-GDSAAGCCCATVCGRTC-3')

frc627-R (5'-TGCTGRTCRCGYAGYTTSAC-3')

S3.4 Polymerase chain reaction program

The PCR mixture consisted of 1 μL of 0.4 μM forward and reverse primers (Microsynth AG), 12.5 μL Sigma-Aldrich REDTaq® ReadyMix™ PCR Reaction Mix, 8.5 μL MilliQ, and 2 μL DNA template (25 μL total volume). The following program was used for the polymerase chain reaction: initial denaturation at 94 °C for 5 min, followed by 40 amplification cycles of denaturation at 94 °C for 30 s, annealing at 57 °C for 1 min, and elongation

at 72 °C for 30 s, with a final elongation step at 72 °C for 10 min. The PCR products were separated using 1.2 % agarose gel electrophoresis at 100 V for 20 min and visualized with a GenePlex Gene View UV Transilluminator. For sequencing, undiluted samples showing an amplification bar (26 samples) and additional samples without an amplification bar (5 samples) were used as controls. Depending on the initial concentration, dilutions or concentrations using a MultiScreenHTS vacuum system were made at 4 ng μL^{-1} in 25 μL .

S3.5 Sequence analysis

To ensure data quality, FastQC (v0.11.7; Andrews, 2010) was used to assess the quality of the raw reads. As the quality of many reads declined towards the end, Trimmomatic (v0.32; Bolger et al., 2014) was employed to trim low-quality bases and short reads with the following parameters SLIDINGWINDOW:4:15 MINLEN:25, resulting in a dataset of sufficient quality. Subsequently, LotuS2 (Özkurt et al., 2022) with *DADA2* (Callahan et al., 2016) were used to identify unique amplicon sequence variants (ASVs) within the cleaned dataset.

Unlike traditional microbial barcodes (e.g. ITS, 16S rRNA, or 18S rRNA), there is no public database containing reference sequences and associated taxonomy for the *frc* gene target region. Therefore, we used RAPPAS (rapid alignment-free phylogenetic placement via ancestral sequences; Linard et al. 2019) to assign taxonomy to the identified ASVs. For this, we queried on November 9th 2023 the UniProtKB database (UniProt Consortium, 2023) with the term ‘Formyl-CoA:oxalate CoA-transferase’ (i.e. *frc*) to get amino acid (AA) sequences related to this gene target. After filtering for appropriate sequence lengths (between 382 and 469 amino acids), a dataset of 4582 bacterial AA sequences was obtained. One sequence per genus was randomly selected, along with an outgroup sequence from the Archeum *Natrarchaeobius chitinivorans*. A multiple sequence alignment of these 186 sequences (122 Pseudomonadota, 51 Actinomycetota, 7 Bacteroidota, 4 Bacillota, 1 Nitrospirota, and 1 Methanobacteriota) was generated using MAFFT with default parameters. The optimal tree model was determined using IQ-TREE2 (Minh et al., 2020) with default parameters and rooted to the outgroup. Subsequently, RAPPAS constructed a phylo-k-mer database using a k-mer size of 5, as recommended by Linard et al. (2019).

The next step involved the placement of representative ASVs obtained from LotuS2. To accomplish this, ASVs nucleotidic sequences were translated into AA sequences using EMBOSS transeq (Rice et al., 2000) with the ‘-frame 6’ argument. Subsequently, the six potential open reading frames were examined, and sequences containing inserted stop codons were discarded, as a complete AA sequence was expected. This process resulted in multiple potential AA sequences for a single ASV (a total of 187 920 AA sequences for 31 320 ASVs). Each of these AA sequences was then placed within the phylogenetic framework using the RAPPAS’ phylo-kmer database.

The RAPPAS output file was then imported into R to build a *phyloseq* object for further analysis (McMurdie and Holmes 2013). We then compared the ASV count table (LotuS2 output) to the taxonomic information linked to unique ASV identifier-based AA sequences (RAPPAS output). Each AA sequences were placed at least once on the reference tree. To determine a unique taxonomic assignment of an ASV based on the phylogenetic placement of its AA sequences, the following approach was employed. If a translated ASV yielded a single AA sequence that was directly placed on a branch leading to a leaf or tip (representing a genus), it was assigned to that genus. For ASVs with multiple AA sequences, the placement with the highest ‘like weight ratio’, as provided by RAPPAS, was considered the most likely. If this placement was at a tip, the ASV was assigned to the corresponding genus. If the placement was on an internal branch, the *phytool* R package (Revell, 2024) was used to extract the subtree containing the placement. The lowest shared taxonomic rank among the genera within this subtree was assigned to the AA sequence, and any lower taxonomic ranks were considered unknown. At this stage, if multiple internal branch taxonomies remained, the most likely was again chosen based on the highest ‘like weight ratio’. This treatment resulted in a *phyloseq* object including 30 345 ASVs belonging to the Bacteria Kingdom.

S3.6 Alpha and beta diversity statistical analysis

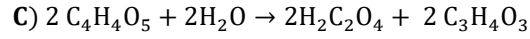
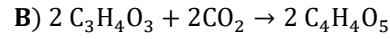
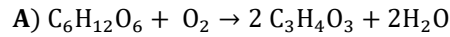
Alpha diversity within samples was assessed by computing the following indices: richness, Shannon index, and Simpson index. To determine significant differences in alpha diversity metrics between sample types, pairwise Wilcoxon rank-sum tests with Benjamini-Hochberg correction for multiple comparisons were performed for each metric. For beta diversity analysis, a distance matrix was computed using the *avgdist()* function in *vegan* (Bray-Curtis method, subsampling size 153 102, which represents the minimum sample count in the dataset). All *p*-values resulting from alpha and beta diversity analyses were adjusted using Benjamini-Hochberg correction for multiple comparisons and the same significance threshold as mentioned above was used for further discussion.

S3.7 Principal Component Analysis

Principal Component Analysis (PCA) was performed to reduce dimensionality and identify patterns in soil biogeochemical properties across samples. The analysis was conducted on a subset of variables related to soil chemistry and nutrient content (variables listed in Table S7 and presented in Fig. S11). Prior to analysis, all variables were standardized, and the PCA was performed on the variable correlation matrix using the *prcomp()* function in R. Samples projected on the plane of the first two principal components were visualized in plots, with sample scores plotted by parent material. Ellipses representing 95 % confidence intervals were added for each

group to illustrate clustering and dispersion. A second plot displays the projections of the variables on the circle of correlations between variables and the first two principal components.

S4: Eq. (S) – Supplementary equations



Eq. (S1). The biosynthesis of oxalic acid from glucose by trees, converting photosynthate into a common low molecular weight organic acid, which can then be loaded into crystal idioblasts for calcium oxalate formation (adapted from Verrecchia et al. 2006). **(A)** Glucose is first oxidised to pyruvate. **(B)** The carboxylation of pyruvate produces oxaloacetate. **(C)** Finally, hydrolysis of oxaloacetate yields acetate and oxalic acid, the latter being transported to crystal idioblasts to precipitate as calcium oxalate.



Eq. (S2). The weathering of limestone (CaCO_3) by carbonic acid (H_2CO_3) draws down carbon dioxide (CO_2) and releases bicarbonate (HCO_3^-) while the subsequent precipitation of secondary CaCO_3 releases CO_2 .

References

- Akpakpan, A. and Akpabio, U.: Evaluation of proximate composition, mineral element and anti-nutrient in almond (*Terminalia catappa*) seeds, Res. J. Appl. Sci., 7, 489–493, <https://doi.org/10.3923/rjasci.2012.489.493>, 2012.
- Alli Smith, Y.: Determination of chemical composition of *Senna siamea* (Cassia leaves), Pak. J. Nutr., 8, 119–121, <https://doi.org/10.3923/pjn.2009.119.121>, 2009.
- Álvarez-Rivera, O. O., Estrada-Medina, H., Jiménez-Osornio, J. J., O'Connor-Sánchez, I. A., Navarro-Alberto, J. A., Ferrer, M. M., Canto-Canché, B., and Tzec-Gamboa, M. D. C.: Differences in oxalate–carbonate pathway of *Brosimum alicastrum* in karst homegarden and forest soils, Soil Sci. Soc. Am. J., 85, 691–702, <https://doi.org/10.1002/saj2.20228>, 2021.
- Andrews, S.: FastQC: a quality control tool for high throughput sequence data, 2010.
- Aragno, M. and Verrecchia, E. P.: The oxalate-carbonate pathway: a reliable sink for atmospheric CO₂ through calcium carbonate biomineralization in ferrallitic tropical soils, in: Microorganisms in Environmental Management: Microbes and Environment, edited by: Satyanarayana, T. and Johri, B. N., Springer Netherlands, Dordrecht, 191–199, https://doi.org/10.1007/978-94-007-2229-3_9, 2012.
- Bolger, A. M., Lohse, M., and Usadel, B.: Trimmomatic: a flexible trimmer for Illumina sequence data, Bioinform., 30, 2114–2120, <https://doi.org/10.1093/bioinformatics/btu170>, 2014.
- Bravo, D., Braissant, O., Cailleau, G., Verrecchia, E., and Junier, P.: Isolation and characterization of oxalotrophic bacteria from tropical soils, Arch. Microbiol., 197, 65–77, <https://doi.org/10.1007/s00203-014-1055-2>, 2015.
- Cailleau, G., Braissant, O., and Verrecchia, E. P.: Turning sunlight into stone: the oxalate-carbonate pathway in a tropical tree ecosystem, Biogeosciences, 8, 1755–1767, <https://doi.org/10.5194/bg-8-1755-2011>, 2011.
- Cailleau, G., Mota, M., Bindschedler, S., Junier, P., and Verrecchia, E. P.: Detection of active oxalate-carbonate pathway ecosystems in the Amazon Basin: Global implications of a natural potential C sink, Catena, 116, 132–141, <https://doi.org/10.1016/j.catena.2013.12.017>, 2014.
- Callahan, B. J., McMurdie, P. J., Rosen, M. J., Han, A. W., Johnson, A. J. A., and Holmes, S. P.: DADA2: High resolution sample inference from Illumina amplicon data, Nat Methods, 13, 581–583, <https://doi.org/10.1038/nmeth.3869>, 2016.
- Chanda, S., Nagani, K., and Parekh, J.: Assessment of quality of *Manilkara hexandra* (Roxb.) Dubard leaf (Sapotaceae): Pharmacognostical and physicochemical profile, Pharmacogn. J., 2, 520–524, [https://doi.org/10.1016/S0975-3575\(10\)80054-9](https://doi.org/10.1016/S0975-3575(10)80054-9), 2010.
- Clerc de SonarcLens, M.: La voie oxalate-carbonate: le cas indien, Master of Science in Biogeosciences, University of Neuchâtel, 61 pp., 2011.
- Dhale, D., Chamle, D., and Panchal, V.: Evaluations of phytochemical constituents and antimicrobial activity of *Butea monosperma* (Fabaceae), J. Phytol., 2, 17–21, 2010.
- Ferro, K. I.: The impact of oxalogenic plants on soil carbon dynamics: formation of a millennium carbon storage as calcium carbonate, PhD thesis, University of Neuchâtel, 2012.
- Friday, E. T., James, O., Olusegun, O., and Gabriel, A.: Investigations on the nutritional and medicinal potentials of *Ceiba pentandra* leaf: A common vegetable in Nigeria, Int. J. Plant Physiol. Biochem., 3, 95–101, 2011.
- Garvie, L. A.: Decay of cacti and carbon cycling, Naturwiss., 93, 114–118, <https://doi.org/10.1007/s00114-005-0069-7>, 2006.
- Garvie, L. A. J.: Decay-induced biomineralization of the saguaro cactus (*Carnegiea gigantea*), Am. Mineral., 88, 1879–1888, <https://doi.org/10.2138/am-2003-11-1231>, 2003.

Hervé, V., Clerc, M., Cailleau, G., Bueche, M., Junier, T., Verrecchia, E., and Junier, P.: Carbonate accumulation in the bark of *Terminalia bellirica*: A new habitat for the oxalate-carbonate pathway, *Geomicrobiol. J.*, 35, 31–39, <https://doi.org/10.1080/01490451.2017.1309087>, 2018.

Ibrahim, J. A., Ayodele, E. A., Jegede, A. I., and Kunle, Y. F.: Comparative studies on *Khaya* A. Juss (Meliaceae) in Nigeria, *Afr. J. Biotechnol.*, 5, 1154–1160, 2006.

Jadhav, V. M.: Herbal medicine: *Syzygium cumini*: a review, *J. Pharm. Res.*, 2, 1212–1219, 2009.

Khalid, M., Akhtar, J., Badruddeen, A. M., and Singh, K.: Pharmacognostical investigation and total phenolic content of *Dalbergia latifolia* (Roxb) bark, *Int. J. Pharmacogn.*, 2, 248–253, [https://doi.org/10.13040/IJPSR.0975-8232.IJP.2\(5\).248-53](https://doi.org/10.13040/IJPSR.0975-8232.IJP.2(5).248-53), 2015.

Linard, B., Swenson, K., and Pardi, F.: Rapid alignment-free phylogenetic identification of metagenomic sequences, *Bioinform.*, 35, 3303–3312, <https://doi.org/10.1093/bioinformatics/btz068>, 2019.

Loeppert, R. H. and Suarez, D. L.: Carbonate and gypsum, in: *Methods of Soil Analysis*, John Wiley & Sons, Ltd, 437–474, <https://doi.org/10.2136/sssabookser5.3.c15>, 1996.

Loeppert, R. H., Hallmark, C. T., and Koshy, M. M.: Routine procedure for rapid determination of soil carbonates, *Soil Sci. Soc. Am. J.*, 48, 1030–1033, <https://doi.org/10.2136/sssaj1984.03615995004800050016x>, 1984.

Malik, R. S., Dutt, D., Tyagi, C. H., Jindal, A. K., and Lakharia, L. K.: Morphological, anatomical and chemical characteristics of *Leucaena leucocephala* and its impact on pulp and paper making properties, *J. Sci. Ind. Res.*, 63, 125–133, 2004.

McMurdie, P. J. and Holmes, S.: phyloseq: An R package for reproducible interactive analysis and graphics of microbiome census data, *PloS One*, 8, 1–11, <https://doi.org/10.1371/journal.pone.0061217>, 2013.

Minh, B. Q., Schmidt, H. A., Chernomor, O., Schrempf, D., Woodhams, M. D., von Haeseler, A., and Lanfear, R.: IQ-TREE 2: New Models and Efficient methods for phylogenetic inference in the genomic era, *Mol. Biol. Evol.*, 37, 1530–1534, <https://doi.org/10.1093/molbev/msaa015>, 2020.

Özkurt, E., Fritscher, J., Soranzo, N., Ng, D. Y. K., Davey, R. P., Bahram, M., and Hildebrand, F.: LotuS2: an ultrafast and highly accurate tool for amplicon sequencing analysis, *Microbiome*, 10, 1–14, <https://doi.org/10.1186/s40168-022-01365-1>, 2022.

Paarakh, P. M.: *Ficus racemosa* Linn. - An overview, *Int. Res. J. Modern. Eng. Technol. Sci.*, 8, 2943–2952, <https://doi.org/10.56726/IRJMETs47797>, 2009.

Pande, J., Padalia, H., Donga, S., and Chanda, S.: Development of quality control parameters for the standardization of *Aegle marmelos* (Roxb) seed, *IJPSR*, 9, 2387–2394, [https://doi.org/10.13040/IJPSR.0975-8232.9\(6\).2387-94](https://doi.org/10.13040/IJPSR.0975-8232.9(6).2387-94), 2018.

Pierantoni, M., Tenne, R., Rephael, B., Brumfeld, V., Casteren, A. van, Kupczik, K., Oron, D., Addadi, L., and Weiner, S.: Mineral deposits in *Ficus* leaves: morphologies and locations in relation to function, *Plant Physiol.*, 176, 1751–1763, <https://doi.org/10.1104/pp.17.01516>, 2018.

Pons, S., Bindschedler, S., Sebag, D., Junier, P., Verrecchia, E., and Cailleau, G.: Biocontrolled soil nutrient distribution under the influence of an oxalogenic-oxalotrophic ecosystem, *Plant Soil*, 425, 145–160, <https://doi.org/10.1007/s11104-018-3573-1>, 2018.

Prakash, O., Srivastava, R., Kumar, R., Mishra, S., and Srivastava, S.: Preliminary pharmacognostic and phytochemical studies on leaves of *Artocarpus heterophyllus*, *Int J. Nat. Prod Mar Bio*, 1, 35–40, 2015.

Randevoson, M. F.: Impacts de la voie oxalate-carbonate sur les caractéristiques édaphiques et organiques des sols forestiers tropicaux (Forêt de Kirindy, Madagascar), PhD thesis, University of Lausanne, 2019.

- Revell, L. J.: phytools 2.0: an updated R ecosystem for phylogenetic comparative methods (and other things), *PeerJ*, 12, 1–75, <https://doi.org/10.7717/peerj.16505>, 2024.
- Rice, P., Longden, I., and Bleasby, A.: EMBOSS: the european molecular biology open software suite, *Trends Genet.*, 16, 276–277, [https://doi.org/10.1016/s0168-9525\(00\)02024-2](https://doi.org/10.1016/s0168-9525(00)02024-2), 2000.
- Rowley, M. C., Estrada-Medina, H., Tzec-Gamboa, M., Rozin, A., Cailleau, G., Verrecchia, E. P., and Green, I.: Moving carbon between spheres, the potential oxalate-carbonate pathway of *Brosimum alicastrum* Sw.; Moraceae, *Plant Soil*, 412, 465–479, <https://doi.org/10.1007/s11104-016-3135-3>, 2017.
- Rowley, M. C., Grand, S., Adatte, T., and Verrecchia, E. P.: A cascading influence of calcium carbonate on the biogeochemistry and pedogenic trajectories of subalpine soils, Switzerland, *Geoderma*, 361, 1–12, <https://doi.org/10.1016/j.geoderma.2019.114065>, 2020.
- Sahri, M. H., Ibrahim, F. H., and Shukor, N. A. A.: Anatomy of *Acacia mangium* grown in Malaysia, *IAWA J.*, 14, 245–251, <https://doi.org/10.1163/22941932-90001326>, 1993.
- Sharawy, S. M.: Numerical taxonomic evaluation of calcium oxalate and calcium carbonate crystals in the leaves of certain *Ficus* species (Moraceae), *Feddes Repert.*, 115, 441–452, <https://doi.org/10.1002/fedr.200411046>, 2004.
- Sharma, N., Singh, S., and Singh, S. K.: Pharmacognostical standardization and preliminary phytochemical investigations on *Acacia auriculiformis* A. Cunn. Ex. Benth stem bark, *Journal of Medicinal Plants*, 5, 398–402, 2017.
- Srivastava, N., Prakash, D., and Behl, H. M.: Biochemical contents, their variation and changes in free amino acids during seed germination in *Terminalia arjuna*, *Int. J. Food Sci. Nutr.*, 48, 215–219, <https://doi.org/10.3109/09637489709012595>, 1997.
- Steinmann, O.: Enquête exploratoire de la voie oxalate-carbonate en milieu karstique et agroforesterie tropicale, Yucatan, Mexique, Master of Science in Biogeosciences, University of Lausanne, Institute of Earth Surface Dynamics, 2020.
- Subramanian, P., Prabhakaran, R., SenthilKumar, M., Babu, K., and Selvaraj, B.: XRD investigation of clay minerals of the Tertiary formations around Panrutti, Cuddalore District, Tamil Nadu, *IJRSR*, 4, 757–760, 2013.
- Sundaram, R., Henderson, R. A., Ayyasami, K., and Stilwell, J. D.: A lithostratigraphic revision and palaeoenvironmental assessment of the Cretaceous System exposed in the onshore Cauvery Basin, southern India, *Cretac. Res.*, 22, 743–762, <https://doi.org/10.1006/cres.2001.0287>, 2001.
- UniProt Consortium: UniProt: the universal protein knowledgebase in 2023, *Nucleic Acids Res.*, 51, D523–D531, <https://doi.org/10.1093/nar/gkac1052>, 2023.
- Verrecchia, E. P., Braissant, O., and Cailleau, G.: The oxalate-carbonate pathway in soil carbon storage: the role of fungi and oxalotrophic bacteria, in: *Fungi in biogeochemical cycles*, vol. 24, edited by: Gadd, G. M., Cambridge University Press, 289–310, 2006.
- Vincent, A. and Violette, S.: Why seawater intrusion has not yet occurred in the Kaluvelli-Pondicherry basin, Tamil Nadu, India, *Hydrogeol. J.*, 25, 1893–1907, <https://doi.org/10.1007/s10040-017-1558-4>, 2017.
- Wallnöfer, B.: The biology and systematics of Ebenaceae: a review, *Ann. Naturhist. Mus. Wien, B Bot. Zool.*, 103, 485–512, 2001.